Algorithm of locating the sphere center imaging point based on novel edge model and Zernike moments for vision measurement

Article *in* Journal of Modern Optics · September 2018

DOI: 10.1080/09500340.2018.1515377

CITATIONS
8

READS
193

4 authors, including:

Yunhui Li
Shanghai University
16 PUBLICATIONS **52** CITATIONS

SEE PROFILE

Zhang Guiyang
Harbin Institute of Technology
7 PUBLICATIONS **39** CITATIONS

SEE PROFILE

Journal of Modern Optics

ISSN: 0950-0340 (Print) 1362-3044 (Online) Journal homepage: https://www.tandfonline.com/loi/tmop20

Algorithm of locating the sphere center imaging point based on novel edge model and Zernike moments for vision measurement

Yunhui Li, Ju Huo, Ming Yang & Guiyang Zhang

To cite this article: Yunhui Li, Ju Huo, Ming Yang & Guiyang Zhang (2019) Algorithm of locating the sphere center imaging point based on novel edge model and Zernike moments for vision measurement, Journal of Modern Optics, 66:2, 218-227, DOI: 10.1080/09500340.2018.1515377

To link to this article: https://doi.org/10.1080/09500340.2018.1515377

Published online: 28 Sep 2018.

JOURNAL OF MODERN OPTICS
2019, VOL. 66, NO. 2, 218–227
https://doi.org/10.1080/09500340.2018.1515377

Taylor & Francis
Taylor & Francis Group

Algorithm of locating the sphere center imaging point based on novel edge model and Zernike moments for vision measurement

Yunhui Li [a], Ju Huo [b], Ming Yang [a] and Guiyang Zhang [a]

[a]School of Astronautics, Harbin Institute of Technology, Harbin, People's Republic of China; [b]School of Electrical Engineering and Automation, Harbin Institute of Technology, Harbin, People's Republic of China

ABSTRACT

High accuracy of locating the sphere center imaging points is crucial for the vision measurement system. This paper investigates the effect of projection projective model on extraction of the sphere center, upon which the sub-pixel edge-location algorithm based on the sphere projection model is proposed. The sphere center projection model is established by analysing the process of sphere imaging, and the sub-pixel edge-location algorithm consisted of the novel edge model and the improved Zernike moment computing is studied. The novel edge model based on the Erf (error function) is adopted for modelling the practical edge part, which obtains the edge distribution points with high precision. Then a closed-form solution of edge locating error compensation is calculated based on Zernike moments. Finally, the proposed method is verified via simulations and experiments. The relevant results show that the proposed method can accurately locate the sphere center imaging point, which further improves the precision and robustness of the vision measurement system.

ARTICLE HISTORY
Received 13 January 2018
Accepted 4 August 2018

KEYWORDS
Vision measurement; spherical target; edge model; Zernike moments; sub-pixel accuracy

1. Introduction

Sign point locating plays an important role in the field of visual measurement, robot vision, and computer graphics, etc. In this sense, the methodologies for extraction of the sign points have attracted considerable attention (*1*–*4*), specially for the spherical targets. Spherical targets are widely used due to the images of spheres contain the characteristic of rotational invariance (*5*,*6*), which overcomes the shortcoming of the planar targets that cannot be observed by all cameras for the large viewing angle and partial occlusion in multi-camera measurement systems. However, in most cases that the center of the spherical image is not the spherical center imaging point unless the spherical center is on the optical axis (*7*,*8*). Therefore, there will exist a deviation between these two centers, which is denoted as the SCIE (Spherical Center Imaging Error). In order to improve the accuracy of the vision measurement, it is of great importance and significance to analyse the perspective projection process of the spherical targets.

During the past few years, much progress has been made in the study on the location of sign points. Ref. (*9*) made analysis of the perspective projection process, the distortion model of the spatial circle projection is established. However, the imaging distortion of a spatial circle is relied on the angle and displacement of the image plane and projection object. Therefore, the range of application is limited to the spatial circles. Literature (*10*) established a distortion error model for the imaging process according to the perspective projection. A law for the distortion error is acquired with some simulations. However, the computational complexity is high, and the pose of the ellipse should be known in the camera coordinate system. Gu et al (*11*). Performed an analysis and simulation for the SCIE by the coincidence of origins of the spherical target coordinate system and the camera coordinate system, which established the variation law of the SCIE and built the error correction model. However, this model is an approximation for the ideal error model, and six spatial positions must be known. In addition, the ratio between the spherical radius and the object distance should be limited to avoid the poor adaptability. Soon afterwards, an expression of accurate analytical of the SCIE is derived; see, for example, (*12*) and reference therein. Although this method has no theoretical error, but the SCIE is affected by the ellipse fitting, image quality and edge location accuracy. In addition, it is hard to ensure that the sphere center imaging point and the ellipse center are collinear.

CONTACT Ming Yang lyaprunov@163.com School of Astronautics, Harbin Institute of Technology, Harbin, People's Republic of China

Another key technique for the locating precision of sphere center imaging point is the sphere image edge-location (*13*). In the edge-location methods (*14*,*15*), moment-based techniques are insensitive to noise, and it is wieldy used. To improve the accuracy of the image edge extraction by employing the moment-based techniques, Tabatabai et al. (*16*) proposed the edge location schemes that use the third-order grey moment and it determined the edge with sub-pixel accuracy. This method provided the edge location in a closed-form and it does not require interpolation or iteration. Additionally, it is invariant to the additive and multiplicative grey level changes. Lyvers et al (*17*). Developed a grey-level moment-based method to determine the location angle and grey-level step height of an edge. These two methods in (*16*,*17*) have a high accuracy but computational costs is large. Ghosal et al. in Ref (*18*). Put forward a sub-pixel location algorithm based on the Zernike orthogonal moments, which acquires a high accuracy with lower computational requirement. However, it is not suitable for small objects. Afterwards, an approach was proposed based on the orthogonal Fourier-Mellin moments (OFMM) to describe and extract small objects in images, of which the details can be seen in (*19*).

In those above mentioned sub-pixel edge-locating methods, an ideal step edge model is used to describe the actual edge, while the focal blur, the cast shadow scenarios, the penumbral blur and uneven illumination distribution are existing in the imaging system. As shown in Figure 3, a deviation occurs between the digital sampling edge and the actual continuous edge. Therefore, an obvious edge location error will be produced with traditional algorithms based on the Zernike moment. To carry out this problem, several edge models have been established based on moment methods. Tabatabai et al. (*16*) proposed an ideal step edge model for the positioning of a greyscale moment. Literature (*17*) presented a three-greyscale edge model for locating spatial moments, where the location accuracy is higher than in the greyscale moment. In Ref (*20*)., Kisworo et al. believed that the ramp-greyscale edge model is more appropriate in certain situations, and experimental tests have shown that the ramp-greyscale edge model has a higher precision than the Tabatabai's edge model. Jian Ye et al. in (*21*) study an edge model based on the Gaussian model. The edge process results show that the accuracy and robustness is higher in the situation where the greyscale distribution is Gaussian rather than a traditional distribution. In addition, Elder et al (*22*). Analysed the imaging process of an edge in the imaging system. On the basis of (*22*), Hagara et al (*23*). Established a blurred edge model based on the Erf (error function) that considers the focal blur, cast shadow scenarios, penumbral blur and uneven illumination distribution. The locating accuracy is higher for the latter model than the other models.

In the available references, the locating algorithms of sphere center imaging point are rely on the positioning center of the spherical image, and the SCIE is related to the positioning accuracy of the spherical image center. For the purpose of getting a high locating accuracy of sphere center in the image without any constraints, in this paper, a directly sub-pixel location approach of sphere center imaging point is proposed based on a locating model of the sphere center imaging point and a sub-pixel edge-location algorithm with improved Zernike moment. The approach aims at the modelling of sphere center imaging point. Then according to the imaging model, a Zernike moment method based on an Erf edge model is utilized to locating the sub-pixel edge of sphere image. The sub-pixel edge points and locating model of sphere center imaging point are utilized to achieve the sphere center in the image.

The remainder of this paper is organized as follows. Section 2 describes the processing of sphere center imaging and reviews the sub-pixel edge locating algorithm. Section 3 presents a locating approach of the sphere center imaging points, which includes a model of sphere center point imaging and a sub-pixel location method for sphere image based improved Zernike moments. Then the simulation and practical experiments are carried out in Section 4 to verify the effectiveness of the given approach. Finally, conclusions are made in Section 5.

2. Preliminaries

2.1. The process of sphere center imaging

The imaging process of a spatial sphere with a standard pinhole camera model is shown in Figure 1, where $Oxyz$ is the camera coordinate system (CCS). O is the optical center; O_uXY is the imaging plane coordinate system; O_u is the cross point of the optical axis and imager plane; f is the focal length of the camera; Γ_2 is the image of the sphere; S_0 and O_2 are the sphere center and projective projection of the center, respectively. S_1 is the center of the ellipse Γ_2; OP_1Q_1 is a conic surface determined by the optical center (O) and the tangent point (P_1,Q_1); Γ_1 is the cone line, and O_1 is the center of Γ_1. The distance of O_2S_1 is defined as SCIE and it is proportional to β.

2.2. Sub-pixel edge-location based on Zernike moment

The ideal step edge model is used to describe the real edge in these traditional methods, but which produce

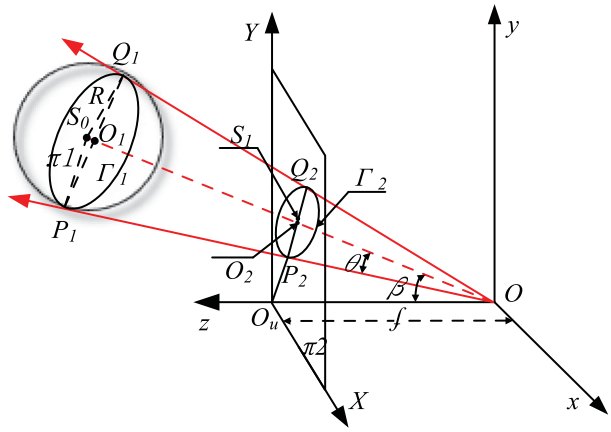

Figure 1. Projective projection model of a sphere.

a correlative error. As shown in Figure 2, an ideal edge model is applied to detect the sub-pixel edge. A normalized ideal 2D edge pattern is established using three basic parameters (h, k, l_D), where h is the background greyscale, k is the greyscale difference, and l_D is the distance from the origin to the theoretical edge. The value φ is the angle between l_D and the x axis, where $\varphi \in (-\pi/2, \pi/2)$. Figure 2(b) shows the model after rotating Figure 2(a) by the angle ϕ.

The Zernike moments of a 2D (two-dimensional) image can be expressed as follows (*20*):

$$A_{nm} = \frac{n+1}{\pi} \iint_{x^2+y^2 \le 1} f(x,y) V^*_{nm}(\rho,\theta) dxdy \quad (1)$$

where $V_{nm}(\rho,\theta)$ is the Zernike polynomial, n and m are the orders of the Zernike moment, '*' denote the conjugate transformation.

The discrete Zernike moments can be written as follows:

$$A_{nm} = \sum_x \sum_y f(x,y) V^*_{nm}(\rho,\theta) \quad x^2+y^2 \le 1 \quad (2)$$

In the polar coordinate system, the Zernike polynomial can be expressed as follows:

$$V_{nm}(\rho,\theta) = \sum_{s=0}^{(n-|m|)/2} \frac{(-1)^s (n-s)! \rho^{n-2s}}{s! \left(\frac{n+|m|}{2}-s\right)! \left(\frac{n-|m|}{2}-s\right)!} e^{jm\theta} \quad (3)$$

According to the computation rule of complex number, we have the following relationship:

$$A'_{nm} = A_{nm} e^{-jm\phi} \quad (4)$$

where $j = \sqrt{-1}$, φ is the rotate angle of image.

From Figure 2, it holds that:

$$\begin{cases} A'_{00} = h\pi + \frac{k\pi}{2} - k\sin^{-1}(l_D) - kl\sqrt{1-l_D^2}, \\ A'_{11} = \frac{2k(1-l_D^2)^{3/2}}{3}, A'_{20} = \frac{2kl_D(1-l_D^2)^{3/2}}{3} \\ A'_{31} = k\sqrt{(1-l_D^2)^3}\left(\frac{4}{5}l_D^2 - \frac{2}{15}\right), \\ A'_{40} = k\sqrt{(1-l_D^2)^3}\left(\frac{16}{15}l_D^3 - \frac{2}{5}l_D\right) \end{cases} \quad (5)$$

The solution of equation (5) is obtained as follows:

$$\begin{cases} l_D = \frac{A_{20}}{A'_{11}}, l_1 = \sqrt{\frac{5A'_{40}+3A'_{20}}{8A'_{20}}}, l_2 = \sqrt{\frac{5A'_{31}+A'_{11}}{6A'_{11}}} \\ k = \frac{3A'_{11}}{2(1-l_D^2)^{3/2}}, h = \frac{A_{00}-\frac{k\pi}{2}+k\sin^{-1}(l)+kl_D\sqrt{1-l_D^2}}{\pi} \end{cases} \quad (6)$$

The sub-pixel edge position of the image can be expressed as follows:

$$\begin{bmatrix} x_s \\ y_s \end{bmatrix} = \begin{bmatrix} x \\ y \end{bmatrix} + l_D \begin{bmatrix} \cos\phi \\ \sin\phi \end{bmatrix} \quad (7)$$

where (x_s, y_s) are the edges of the sub-pixel coordinates and (x, y) indicates that the Sobel operator edge detection is used to obtain the pixel coordinates.

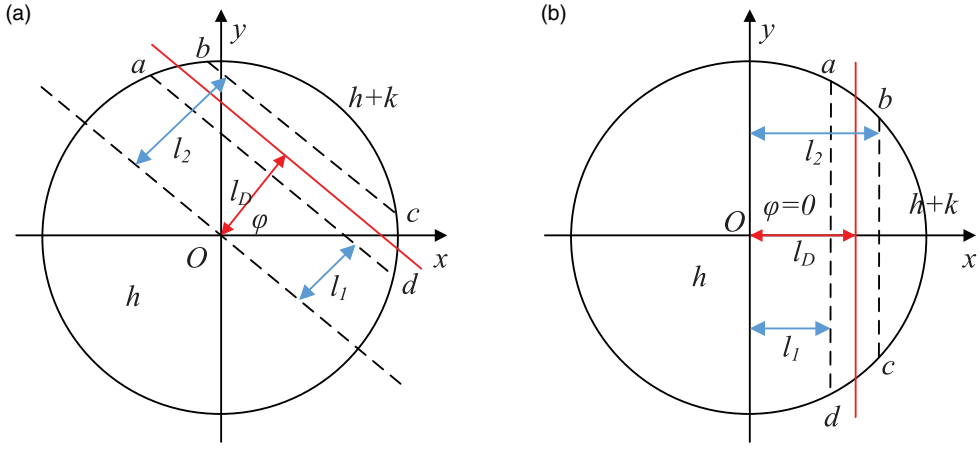

Figure 2. Normalized ideal 2D edge model. (a) Original edge model (b) The edge model after rotating.

Assuming that the Zernike template is N × N. And considering the amplification effect of the template, formula (7) should be rewritten as follows:

$$\begin{bmatrix} x_s \\ y_s \end{bmatrix} = \begin{bmatrix} x \\ y \end{bmatrix} + \frac{N}{2} l \begin{bmatrix} \cos\phi \\ \sin\phi \end{bmatrix} \tag{8}$$

Therefore, compared with the spatial moments method, a higher detection efficiency is observed because the Zernike moments can locate the sub-pixel edge using only A_{00}, A_{11}, and A_{20}.

The above descriptions indicate a certain problems that the ideal 2D edge model is used to locate the sub-pixel edge of an image. The analysis would be proceed in the next section.

3. Locating approach of the sphere center imaging point

In order to decrease the SCIE without other constrains for the spatial sphere, a new locating approach is proposed in this section. It can be divided into two parts, the first is the mathematic model of sphere center imaging point, and the second is the sub-pixel edge-location of the sphere image according to the projective projection mode.

3.1. The proposed model of sphere center imaging point

Based on the process of the projective projection of a sphere in section 2, the sphere center imaging point can be described as follows:

As shown in Figure 1, the vector $\mathbf{OS}_0$ is defined as $\mathbf{OS}_0 = (\cos\alpha, \cos\beta, \cos\gamma)$, with $\cos^2\alpha + \cos^2\beta + \cos^2\gamma = 1$. $P(x, y, z)$ is a point on the cone, θ is the semi vertical angle, and the point P satisfies:

$$\mathbf{OP} \cdot \mathbf{OS}_0)/|\mathbf{OP}| = \cos\theta \tag{9}$$

Expanding formula (9) and simplifying it, we can obtain the following:

$$\frac{\cos\alpha}{\cos\gamma}x + \frac{\cos\beta}{\cos\gamma}y + z - \frac{\cos\theta}{\cos\gamma}\sqrt{x^2 + y^2 + z^2} = 0 \tag{10}$$

Substituting the three parameters $\lambda = \cos\alpha/\cos\gamma$, $\mu = \cos\beta/\cos\gamma, \sigma = \cos\theta/\cos\gamma$ into equations (9) and (10), it can be simplified as follow:

$$\lambda x + \mu y + z - \sigma\sqrt{x^2 + y^2 + z^2} = 0 \tag{11}$$

The conic surface intersect the image plane at $z = f$. Therefore, we can obtain the parameter equation of the conic surface in the CCS:

$$f(x, y) = \lambda x + \mu y - \sigma\sqrt{x^2 + y^2 + f^2} + f = 0 \tag{12}$$

The relationship of the pixel coordinate (u, v) (in pixels) and the image coordinate (x, y) (in millimetres) can be expressed as follow:

$$\frac{x}{f} = \frac{u - u_0}{f_x}, \frac{y}{f} = \frac{v - v_0}{f_y} \tag{13}$$

where f is the focal length of the camera; $f_x = f/dx$ and $f_y = f/dy$ (dx and dy are the vertical and horizontal imager pixel sizes, respectively); and (u_0, v_0) is the principal point. Then, the following equation (in pixels) is obtained:

$$\lambda\left(\frac{u - u_0}{f_x}\right) + \mu\left(\frac{v - v_0}{f_y}\right) - \sigma\sqrt{\left(\frac{u - u_0}{f_x}\right)^2 + \left(\frac{v - v_0}{f_y}\right)^2 + 1} + 1 = 0 \tag{14}$$

We can use the least squares method to solve equation (14), and the optimal solutions of (λ, μ, σ) are obtained. The define of parameters (λ, μ, σ) can be used to solve $\cos\alpha$, $\cos\beta$, $\cos\gamma$ and $\cos\theta$, which $\cos^2\alpha + \cos^2\beta + \cos^2\gamma = 1$.

Because the line from O to $O2$ can be expressed as follow:

$$\frac{x}{\cos\alpha} = \frac{y}{\cos\beta} = \frac{z}{\cos\gamma} \tag{15}$$

The plane π_2 can be written as follow:

$$z = f \tag{16}$$

Thus, the imaging center coordinate of the sphere can be given as:

$$x = \frac{\cos\alpha}{\cos\gamma}f, y = \frac{\cos\beta}{\cos\gamma}f, z = f \tag{17}$$

From the formulas (14), (17) and the definition of parameters (λ, μ, σ), we get a relationship between the locating accuracy of sphere center imaging point (x, y) and the sphere projective projection edge point (u, v). Therefore, in order to obtain the high locating accuracy of (x, y). The locating process can be divided into two parts: the camera intrinsic parameters calibrate and the sub-pixel edge of the sphere image extract. For the intrinsic parameters, we employ the Zhang's calibration method (*24*). For the sub-pixel edge extract, we propose a sub-pixel edge-locating algorithm with edge blur compensation to extract the sub-pixel edge. The details on which is demonstrated in the later section.

3.2. The algorithm of Zernike moments sub-pixel edge-location with edge blur compensation

The edge greyscale distribution of sphere image is nonuniform because of the spherical imaging characteristic, imaging angle and uneven illumination distribution. Thus, if the edge of the spherical image is located using these edge models mentioned in the section 1, the error is larger. For this reason, this article establishes an edge model combined with the spherical imaging greyscale distribution and the Erf, and the sub-pixel edge is located based on the Zernike moment combined with the proposed edge model (Figure 3).

The focal blur and penumbral blur can be modelled using a Gaussian blur kernel (*18*):

$$g(x,y,\sigma_b)=\frac{1}{2\pi\sigma_b^2}e^{-(x^2+y^2)/2\sigma_b^2} \tag{18}$$

The integration of the Gaussian function is the Erf (cumulative distribution function):

$$erf(x)=\frac{2}{\sqrt{\pi}}\int_0^x e^{-t^2}dt \tag{19}$$

Ref. (*23*) proposed that the edge can be modelled using an Erf with a mean of l and variance of σ as follow:

$$f_1(x)=\frac{k}{2}\left(erf\left(\frac{x-l}{\sqrt{2}\sigma_b}\right)+1\right)+h \tag{20}$$

Considering that the noise $n(x,y)$ of the sensor is a random variable with a mean of 0 and variance of s_n, Elder et al. (*22*) analysed the process of the edge imaging and proposed an edge model as follow:

$$f(x)=\frac{k}{2}\left(erf\left(\frac{x-l}{\sqrt{2}\sigma_b}\right)+1\right)+h+n(x,y) \tag{21}$$

In this paper, an edge model is established based on the fact that the characteristic greyscale distribution does not always meet the same rule. Under the condition of no sensor noise, we obtain the following:

$$f_{erf}(x,x_i,y_i)=\begin{cases}h & x\le l_1(x_i,y_i)\\ h+\frac{k}{2}\left(erf\left(\frac{x-(l_1+l_2)/2}{\sqrt{2}\sigma_b(x_i,y_i)}\right)+1\right) & l_1(x_i,y_i)\\ & <x<l_2(x_i,y_i)\\ h+k & x\ge l_2(x_i,y_i)\end{cases} \tag{22}$$

where $\sigma_b(x,y)$ describe the standard deviation of the edge point (x,y) with the edge greyscale distribution. The light distribution and the imaging angle are different, and the edge image of the spherical target is diverse in different directions. Therefore, $\sigma_b(x_i,y_i)$ is a function of x_i and y_i, where $i=1,\cdots,8$, and the mean of the spherical target image is divided into 8 neighbourhoods. Then, using the parametric estimation theory (*25*), the variance of the image edge distribution can be estimated.

According to the proposed edge model in this article, the Zernike moment of the image can be recalculated as follows:

$$\begin{cases}A'_{00}=h\pi+\Delta k\left[\arcsin(l_1)-\arcsin(l_2)\right.\\ \left.+l_1\sqrt{1-l_1^2}-l_2\sqrt{1-l_2^2}\right]\\ +k\left[\frac{\pi}{2}-l_2\sqrt{1-l_2{}^2}-\arcsin(l_2)\right]\\ A'_{11}=\frac{2\Delta k}{3}\left[\sqrt{(1-l_1^2)^3}-\sqrt{(1-l_2^2)^3}\right]\\ +\frac{2k}{3}\sqrt{(1-l_2^2)^3}\\ A'_{20}=\frac{2kl_2\sqrt{(1-l_2^2)^3}}{3}\\ -\frac{2\Delta k\left(l_1^3\sqrt{1-l_1^2}-l_2^3\sqrt{1-l_2^2}-l_1\sqrt{1-l_1^2}\right)+l_2\sqrt{1-l_2^2}}{3}\\ A'_{31}=\frac{4\Delta k}{15}\left[\sqrt{1-l_1^2}(2-3l_1^4+l_1^2)\right]\\ -\frac{2\Delta k}{3}\left(\sqrt{(1-l_1^2)^3}-\sqrt{(1-l_2^2)^3}\right)\\ -\frac{2k}{15}\sqrt{1-l_2^2}(6l_2^4-7l_2^2+1)\end{cases} \tag{23}$$

where l_1 is the boundary from background to edge part; l_2 is the boundary from edge to foreground; h is the background grayscale; k is the greyscale difference between foreground and background; $\Delta k$is the greyscale average value of edge region.

Because A'_{00}, A'_{11}, A'_{20}, and A'_{31} can be acquired with equation (23), and substituted into formula (24), we

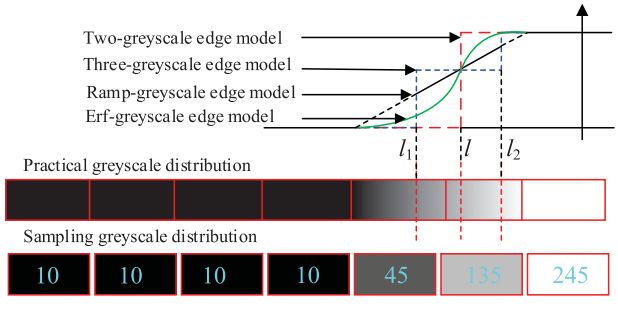

Figure 3. Greyscale distribution of a continuous edge and digital edge.

obtain the sub-pixel edge l_m with Erf edge model as following:

$$l_m = \frac{A'_{20}}{A'_{11}} = \frac{\left(1-\frac{\Delta k}{k}\right) l_2(1-l_2^2)\sqrt{1-l_2^2} + \frac{\Delta k}{k} l_1(1-l_1^2)\sqrt{1-l_1^2}}{\frac{\Delta k}{k}\sqrt{(1-l_2^2)^3} + \left(1-\frac{\Delta k}{k}\right)\sqrt{(1-l_2^2)^3}} \tag{24}$$

where Δk is the average value of the edge transition section. However, the function is nonlinear between Δk and the actual edge l_D because of the focal blur, cast shadow scenarios, penumbral blur and uneven illumination distribution. In this article, we set.

$$l_D = f(\Delta k) \tag{25}$$

where $l_1 \le l_D \le l_2$. Therefore, $0 \le \Delta k = \frac{k}{2}\int_{l_1}^{l_D}\left(1+erf\left(\frac{x-(l_1+l_2)/2}{\sqrt{2}\sigma_b(x_i,y_i)}\right)\right)dx \le \frac{k}{2}(l_2-l_1)$. According to the constraints of the actual image edge, $\frac{k}{2}(l_2-l_1) = \Delta k$ is chosen; hence, l_D can be calculated using numerical methods.

Furthermore, the error introduced by the ideal two-greyscale step model is as follows:

$$E(l_1,l_2,k,\Delta k) = l_m - l_D = \frac{\left(1-\frac{\Delta k}{k}\right) l_2(1-l_2^2)\sqrt{1-l_2^2} + \frac{\Delta k}{k} l_1(1-l_1^2)\sqrt{1-l_1^2}}{\frac{\Delta k}{k}\sqrt{(1-l_2^2)^3} + \left(1-\frac{\Delta k}{k}\right)\sqrt{(1-l_2^2)^3}} - f(\Delta k) \tag{26}$$

The location error using the ideal step model can be compensated with formula (26).

The point (u, v) of sub-pixel edge of sphere image can be extracted by using formulas (24).

According to the deduced of section 3.1 and 3.2, the sphere center imaging point can be calculated using formulas (14), (17), (24) and the definition of (λ, μ, σ). In summary, the procedure of the proposed as follow (Figure 4):

4. Experiment and analysis

4.1. Comparison of the sub-pixel edge-location algorithms

The location methods based on moments include the Grey Moment (GM), Spatial Grey Moment (SGM), Zernike Orthogonal Moment (ZOM), Fourier-Mellin (OFFM) and Partial Area Effect (PAE) (*26*). These methods will be investigated, and the best adaptive one to the complicated lighting environment will be identify. In this article, a comparison of the accuracy and robustness of these five methods will be performed, and then, the comparison will be proceed between the improved ZOM and traditional ZOM in the practical experimental.

4.1.1. Simulation experiment

To compare the accuracy and robustness of the different methods for sub-pixel edge location, one circle target is generated by computer. MATLAB 2017a is applied in the simulation experiment. The region of interest (ROI) is fast extracted by adapting the methods for the coarse edge location. Then, the sub-pixel location experiments for the edge of the ROI is extracted with the methods SGM, ZOM, OFFM, PAE and IZOM, and the results are listed in Table 1. The parameters are set as (1) repetitions: 1000; (2) transverse: 7.8255; (3) semi-minor axis: 6.1008; (4) center of circle: (288.5772, 251.9932); (5) steering angle of ellipse: 0°; (6) Gaussian noise (u,v): (0,0.0001). For the signal-to-noise ratio (SNR) of the synthetic image it is defined as $SNR = 20\lg(k/\sigma)dB$, where k is a greyscale contrast of foreground and background, and σ is the power of standard deviation of the added random noise.

The edge fitting accuracy of the ellipse for the 5 methods is shown in Table 1 under different SNR conditions. Table 1 shows the following:

Table 1. Fitting error of the ellipse target under different SNRs (Unit: pixel).

Algorithm	80 dB	50 dB	40 dB	30 dB	20 dB
SGM	0.0807	0.0812	0.0815	0.0830	0.0837
ZOM	0.0807	0.0816	0.0827	0.0834	0.0890
OFMM	0.0807	0.0816	0.0827	0.0834	0.0890
PAE	0.0509	0.0532	0.0596	0.1644	–
Proposed	0.0537	0.0542	0.0564	0.0671	0.0855

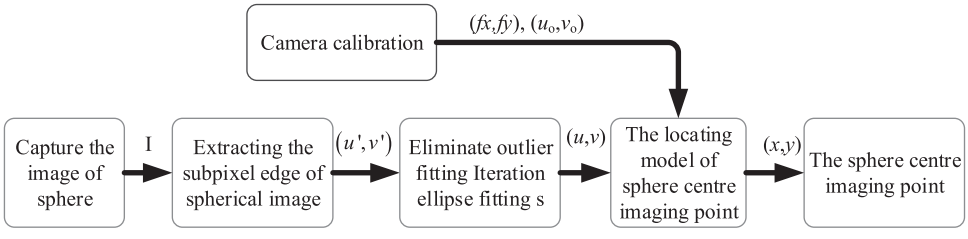

Figure 4. The locating diagram of sphere center imaging point.

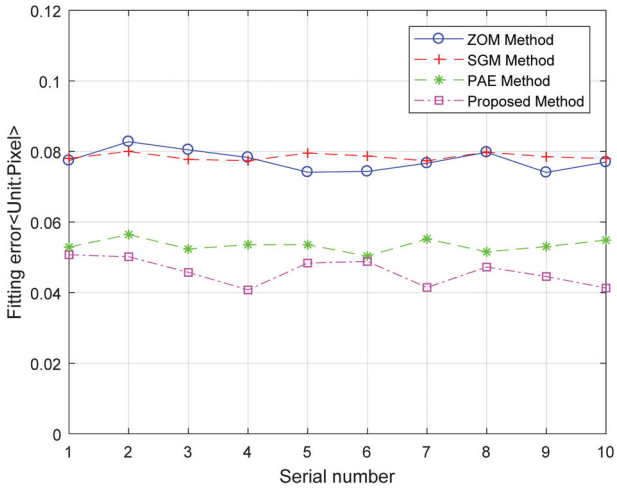

Figure 5. Locating error of the edge point when the SNR is 40 dB.

(1) The PAE has the highest location accuracy when the noise is below 40 dB;
(2) The location accuracy of the proposed method is greater than that of the SGM and ZOM;
(3) The proposed method has a better robustness than the PAE because the ZOM is integration operators, thus, the proposed method is not as sensitive to noise;
(4) The location result of the ZOM and OFMM are the same because they are mathematically equivalent.

Figure 5 shows the root mean square (RMS) of the edge locating error of 10 pictures with a SNR of 40 dB. Figure 5 shows the following:

(1) The SGM has a lower location accuracy than the other models, with the max error reaching 0.08 pixels, although the robustness is the greatest;
(2) The PAE has the greatest balance between the location accuracy and robustness but is unsuitable under the conditions of strong noise;
(3) The accuracy of the proposed method is the highest but the robustness is worse than that of the PAE.

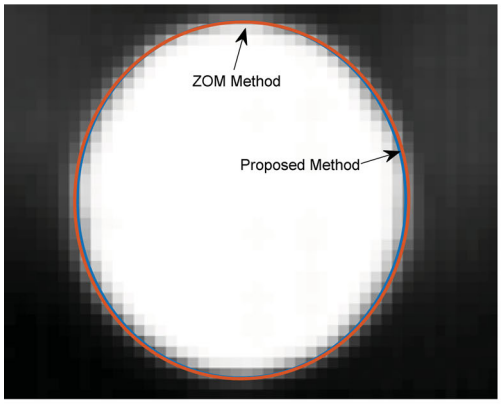

(b)

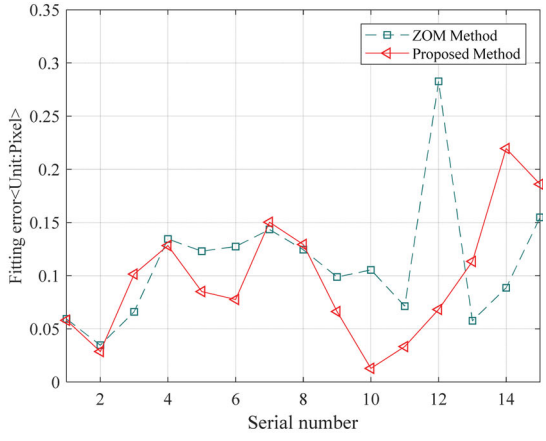

(b)

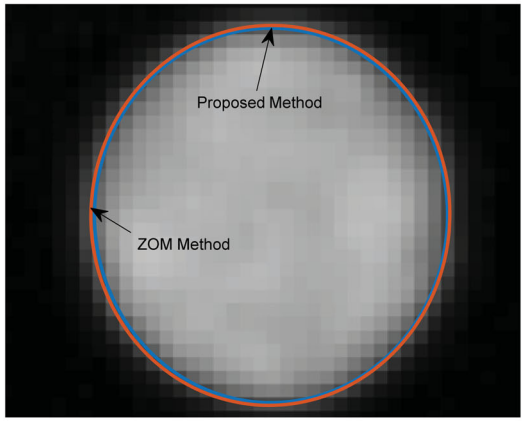

(c)

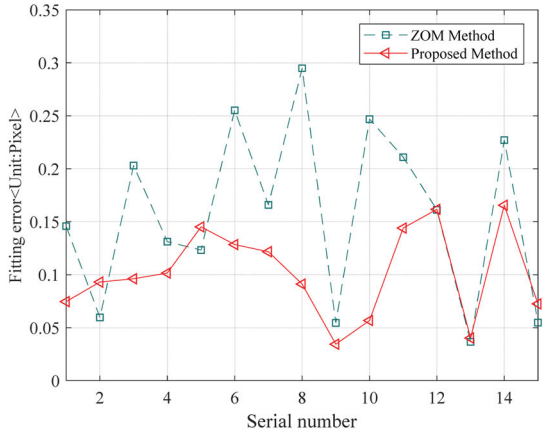

(d)

Figure 6. Typical image captured in the real experiment and the results of the sub-pixel edge locating.

(4) According to Table 1 and Figure 6, the location accuracy of the PAE is significantly decreased when the SNR is less than 40 dB, and if the SNR is less than 20 dB the location cannot be found. Therefore, in general, the proposed method has the best locating accuracy and robustness.

4.1.2. Practical experiment

To verify the locating performance of the proposed sub-pixel locating method for a spherical target with an infrared reflective material, a camera (Mikrotron Germany, MC3010) is used with the following parameters: sensor size of 1680×1710, pixel size of $8\,\mu$m, an AF Zoom-Nikkor 24–85mm/1:2.8–4D lens, and an infrared light source wavelength $\lambda = 850$ nm. The captured image and locating results are shown in Figure 6.

Figure 6(b) and (d) show the results of the target sub-pixel locate using the ZOM and proposed sub-pixel method in this article. The error is the minimum distance between the edge point and the ellipse that obtained through iterative fitting method. Figure 6 shows the following:

(1) The location accuracy of the proposed sub-pixel algorithm and the ZOM are equivalent for the uniform illumination distribution and small SNR as shown in Figure 6(a) and (b).
(2) The location result obtained for the proposed sub-pixel algorithm is better for the uneven greyscale distribution as shown in Figure 6(c) and (d);

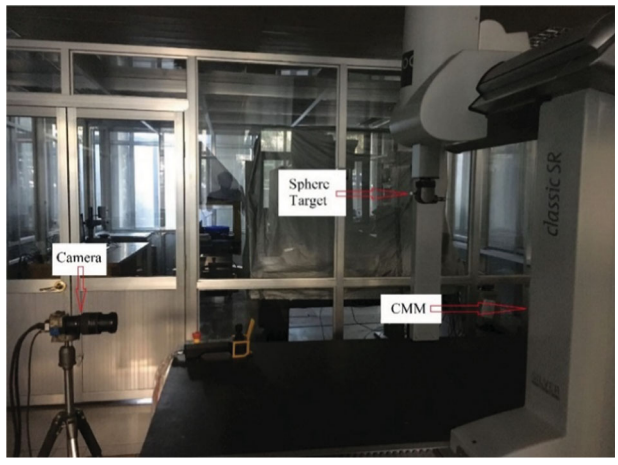

Figure 7. The setup of real camera calibration experiment.

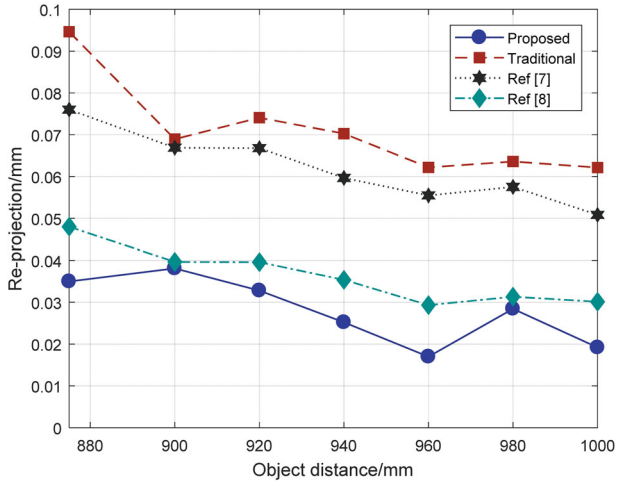

Figure 8. The RMS of re-projective error in each layer.

4.2. Comparison of the sphere center location algorithm for the sphere target

In this section, the proposed sub-pixel location algorithm is combined with the projective model of a sphere center imaging point. The infrared light source wavelength λ is 850 nm; and the cooperative target is composed of infrared reflective material with a diameter of $d = 12.7$ mm. The reflective coating is 850 nm 3M7610. The coordinate measuring machine (CMM) is a Hexagon Global SR 09.20.08, and the measurement range is 900 mm × 2000 mm × 800 mm, the distinguishability is 0.2 μm, and the measurement accuracy is 0.8+L/400 μm (L is the measurement length, and mm is the unit) (Figure 7).

The camera is adjusted, and the FOV is set to 240 mm × 210 mm × 100 mm. The sphere target is attached to the measuring head of the CMM, and the space of vertical the optical axis is divided into 7 layers. Twenty calibration points are arranged in each layer by control of the CMM. The center of the sphere imaging point is extracted using the method in Ref (*7*), Ref (*8*), the traditional algorithm (take no account of SCIE) and the proposed in this paper. The camera is calibrated via a combination of the extracted center and Zhang's method (*24*). The resulting RMS of the re-projective error in object space in each layers calibration is shown in Figure 8. The re-projective error distribution in 3D space and image space is shown in Figure 9. The intrinsic parameters of the camera are acquired with the Zhang's method under 140 calibration points.

According to Figure 8, the analysis results are as follows:

(1) The location accuracy of the sphere center imaging point using the proposed method is higher than that of the another algorithm;
(2) The locating accuracies are 0.0946 and 0.0381 mm traditional and proposed, respectively; thus, the location accuracy of the approach in this paper improves about three times;

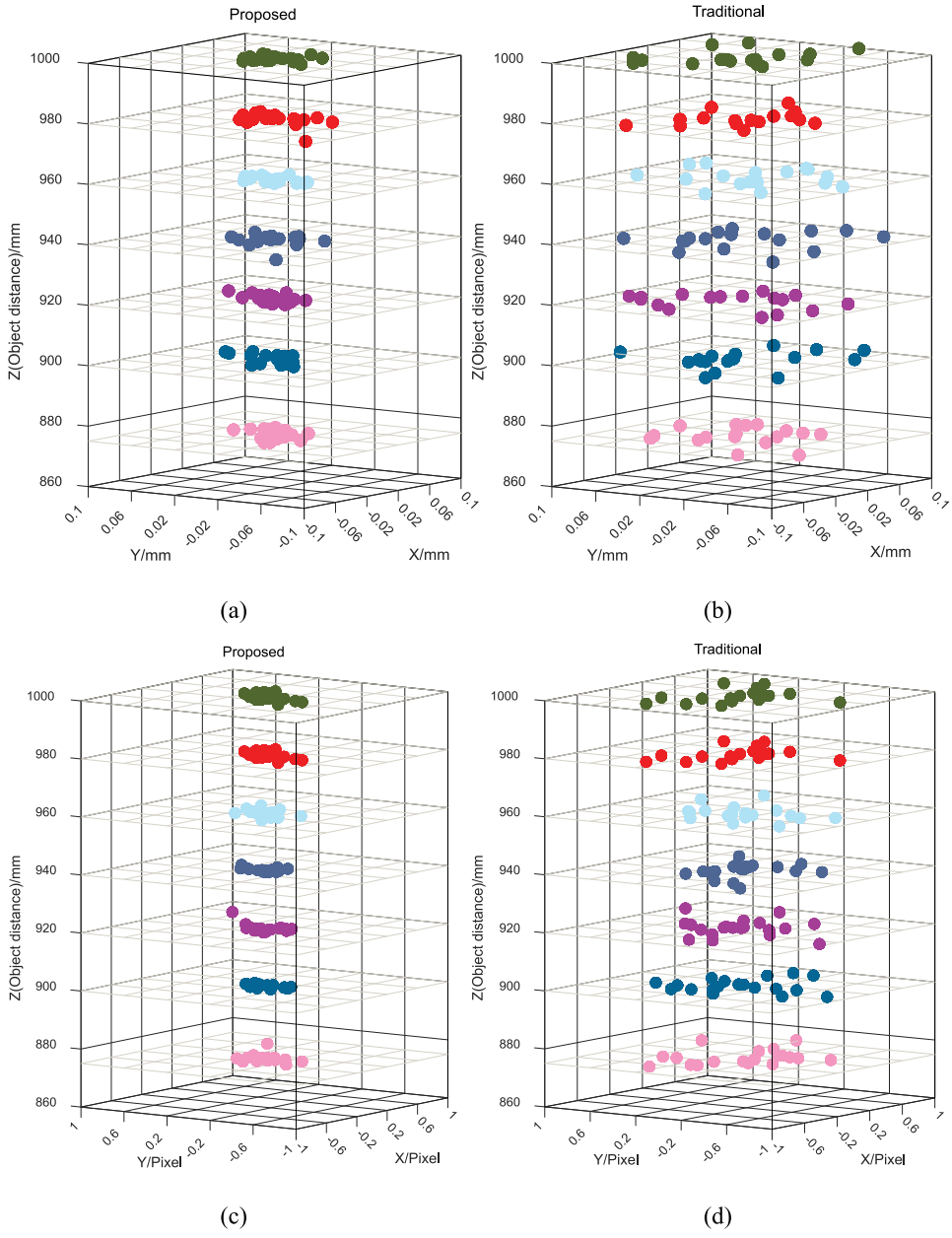

Figure 9. Re-projective error distribution in 3D space and image space.

(3) When the object distance is 875mm, the RMS error is bigger than other object distances except proposed method in this paper. The reason is the edge blur compensation be take into the method.

According to Figure 9, the analysis results are as follows:

(1) The re-projection error in pixels is decrease from 1pixel to 0.6pixel, except the outliers;
(2) The error distribution of proposed method is more concentrated than the traditional, wherever in the 3D space or image space. Therefore, the robustness is significantly increased;
(3) The sphere location error is different between the simulation and practical experiment because the actual edge greyscale distribution does not conform to the characteristics of a sphere projection because of the non-uniform lighting effect. Even so, the effectiveness and rationality are still certified by the data shown in Figure 9.

5. Conclusions

A method of locating a sphere center imaging point is proposed based on a novel sphere center projective model and an improved sub-pixel edge-locating algorithm.

Combining with the sphere projection projective process and spatial geometry, the sphere center projective model is constructed. The new edge model is established based on Erf function in the different directions, and the improved Zernike orthogonal moment with the Erf edge model is used to locate the sub-pixel edge. Hence, the imaging point of the sphere center is located by using the proposed approach. Finally, the experimental results proved the location accuracy and robustness of sphere center imaging point of the proposed method is higher than that of the traditional algorithms under the complicated illumination terms.

Additionally, the edge model is complex and the computation is much larger than that of the ZOM. Therefore, as future works in algorithm effective aspect, when the lighting distribution of the sphere image is different, the edge model should be self-adaption change.

Disclosure statement

No potential conflict of interest was reported by the authors.

Funding

This work was supported by the National Natural Science Foundation of China [grant number 61473100], [grant number 61021002].

ORCID

Yunhui Li http://orcid.org/0000-0002-3562-3406
Guiyang Zhang http://orcid.org/0000-0001-6485-2710

References

(1) Nichols, J.K.; Sena, M.P.; Ju, J.L.; O'Reilly, O.M.; Feeley, B.T.; Lotz, J.C. *Comput. Method Biomech Biomed. Eng.* **2017**, *20*, 1289–1298.
(2) Li, Y.; Xu, L.P.; Jin, H.B.; Zou, J.W.J. *Mod. Opt.* **2016**, *63*, 245–251.
(3) Cui, J.S.; Huo, J.; Yang, M.J. *Mod. Opt.* **2016**, *63*, 835–846.
(4) Huo, J.; Zhang, G.Y.; Yang, M.; Cui, J.S. *J. Mod. Opt.* **2018**, *65*, 331–341.
(5) Fan, S.H. The Information Engineering University, *Ph.D. Thesis*, Zhengzhou, People's Republic of China, **2006**.
(6) Zhang, Z.Y. *IEEE Trans. Pattern Anal. Mach. Intell.* **2004**, *26*, 892–899.
(7) Zhang, H.; Wong, K.K.; Zhang, G.Q. *IEEE Trans. Pattern Anal. Mach. Intell.* **2007**, *29*, 499–502.
(8) Cui, J.S.; Huo J.; Yang, M. *Opt.* **2014**, *125*, 6570–6575.
(9) Heikkila, J.; Silven, O.C. *Proc. IEEE CVPR* **1997**, *1*, 1106–1112.
(10) Wei, Z.Z.; Zhang, G.J. *Chin. J. Sci. Instrum.* **2003**, *24*, 160–164.
(11) Gu, F.F; Zhao, H.; Bu, P.H. *Acta Opt. Sin.* **2012**, *32*, 209–215.
(12) Liu, S.G.; Song, X.X.; Han, Z.Z. *Opt. Precis. Eng.* **2016**, *24*, 1861–1870.
(13) Sun, J.H; He, H.B.; Zeng, D.B. *IEEE Sens. J.* **2016**, *16*, 1–14.
(14) Fabijanska, A. *Int. J. Appl. Math. Comput. Sci.* **2012**, *22*, 695–710.
(15) Health, A.; Sarkar, S.; Sanocki, T. *Comput. Vis. Image Underst.* **1998**, *69*, 38–54.
(16) Tabatabai, A.J.; Mitchell, R. *IEEE Trans. Pattern Anal. Mach. Intell.* **1984**, *6* (2), 188–201.
(17) Lyvers, E.P.; Mitchell, R.; Akey, M.L. *IEEE Trans. Pattern Anal. Mach. Intell.* **1989**, *11*, 1293–1309.
(18) Ghosal, R.M.S. *IEEE Trans. Pattern Anal. Mach. Intell.* **1992**, *1*, 413–416.
(19) Tan, J.B.; Ao, L.; Cui, J.W. *Image Vis. Comput.* **2008**, *26*, 563–569.
(20) Kisworo, M.; Venkatesh, S.; West, G. *IEEE Trans. Pattern Anal. Mach. Intell.* **1994**, *16*, 405–410.
(21) Ye, J.; Fu, G.K.; Upendra, P. *Image Vis. Comput.* **2005**, *23*, 453–467.
(22) Elder, J.H.; Zucker, S.W. *IEEE Trans. Pattern Anal. Mach. Intell.* **1998**, *20* (7), 699–716.
(23) Hagara, M.; Kulla, P. *Radio Eng.* **2011**, *20*, 516–524.
(24) Zhang, Z.Y. *IEEE Trans. Pattern Anal. Mach. Intell.* **2000**, *22* (11): 1330–1334.
(25) Scott, D.W. John Wiley & Sons, **2015**.
(26) Trujillo-Pino, A.; Krissian, K.; Alemán-Flores, M. *Image Vis. Comput.* **2013**, *31*, 72–90.